

Field Induced Order and Spin Waves in the Pyrochlore Antiferromagnet $\text{Tb}_2\text{Ti}_2\text{O}_7$

K.C. Rule,¹ J.P.C. Ruff,¹ B.D. Gaulin,^{1,2} S.R. Dunsiger,¹ J.S. Gardner,^{3,4} J.P. Clancy,¹
M.J. Lewis,¹ H.A. Dabkowska,¹ I Mirebeau,⁵ P. Manuel,⁶ Y. Qiu,^{4,7} and J.R.D. Copley⁴

¹*Department of Physics and Astronomy, McMaster University, Hamilton, Ontario, L8S 4M1, Canada*

²*Canadian Institute for Advanced Research, 180 Dundas St. W., Toronto, Ontario, M5G 1Z8, Canada*

³*Brookhaven National Laboratory, Upton, New York 11973-5000, USA*

⁴*National Institute of Standards and Technology,
100 Bureau Dr., Gaithersburg, MD, 20899-8562, U.S.A.*

⁵*Laboratoire Leon Brillouin, CEA-CNRS, CE-Saclay, 91191 Gif-sur-Yvette, France*

⁶*ISIS Facility, Rutherford Appleton Laboratory, Didcot, Oxon, OX11 0QX, United Kingdom.*

⁷*Department of Materials Science and Engineering,
University of Maryland, College Park, MD, 20742, USA*

High resolution time-of-flight neutron scattering measurements on $\text{Tb}_2\text{Ti}_2\text{O}_7$ reveal a rich low temperature phase diagram in the presence of a magnetic field applied along [110]. In zero field at $T=0.4$ K, $\text{Tb}_2\text{Ti}_2\text{O}_7$ is a highly correlated cooperative paramagnet with disordered spins residing on a pyrochlore lattice of corner-sharing tetrahedra. Application of a small field condenses much of the magnetic diffuse scattering, characteristic of the disordered spins, into a new Bragg peak characteristic of a polarized paramagnet. At higher fields, a magnetically ordered phase is induced, which supports spin wave excitations indicative of continuous, rather than Ising-like spin degrees of freedom.

PACS numbers: 75.25.+z, 75.40.Gb, 75.40.-s

Geometrical frustration is a central theme in contemporary condensed matter physics, as it allows the possibility of exotic ground states¹. Geometries which support magnetic frustration typically involve edge and corner shared triangles and tetrahedra, and these are common in nature. Pyrochlore magnets, with magnetic moments localized at the vertices of a cubic network of corner-sharing tetrahedra, have played a prominent role in this field. Many such systems exist with varied magnetic interactions and anisotropies expressed by real materials.

Idealized systems comprised of classical spins which interact on the pyrochlore lattice are reasonably well understood. Antiferromagnetically-coupled Heisenberg spins are known to have a disordered ground state on the pyrochlore lattice^{2,3,4}. Spins with local [111] Ising anisotropy, such that moments are constrained to point into or out of the tetrahedra, have been extensively studied for both antiferromagnetic and ferromagnetic coupling^{5,6}. Interestingly, it is known that if the local anisotropy is sufficiently strong, ferromagnetic exchange leads to a disordered “spin ice” ground state, while antiferromagnetic exchange gives rise to a $\mathbf{Q}=0$, non-collinear Néel ordered state.

The rare-earth titanate pyrochlores, with the chemical composition $\text{A}_2\text{Ti}_2\text{O}_7$, where the A site is a trivalent rare-earth ion surrounded by a (distorted) cube of eight O^{2-} ions and Ti is in its non-magnetic Ti^{4+} state, have been of particular interest with regard to these latter calculations. The crystal field states of rare-earth ions Ho^{3+} , Dy^{3+} , and Tb^{3+} within $\text{A}_2\text{Ti}_2\text{O}_7$ are such that local [111] Ising anisotropy of the moments is expected^{7,8}.

As the exchange interactions are relatively weak, and the moment sizes are relatively large, the appropriate starting point Hamiltonian for a discussion of these materials is⁵:

$$\mathcal{H} = - \sum_{\langle i,j \rangle} J_{ij} \mathbf{S}_i^{z_i} \cdot \mathbf{S}_j^{z_j} \quad (1)$$

$$+ D_{\text{nn}}^3 \sum_{i > j} \frac{\mathbf{S}_i^{z_i} \cdot \mathbf{S}_j^{z_j}}{|\mathbf{R}_{ij}|^3} - \frac{3(\mathbf{S}_i^{z_i} \cdot \mathbf{R}_{ij})(\mathbf{S}_j^{z_j} \cdot \mathbf{R}_{ij})}{|\mathbf{R}_{ij}|^5}$$

where z_i denotes the local Ising axis. Tb^{3+} in $\text{Tb}_2\text{Ti}_2\text{O}_7$ displays a ground state and 1st excited state doublet, separated by only about $\hbar\omega \sim 1.5$ meV, with higher energy singlet states observed by inelastic neutron scattering at $\hbar\omega \sim 10.5$ and 14.5 meV⁹. The moment associated with the ground state doublet is roughly $5 \mu_B$ ⁷, but it is known to be sensitive to the precise oxygen coordination. A perfect cube of O^{2-} around the Tb^{3+} gives rise, for example, to a non-magnetic doublet.

The magnetic ground state of $\text{Tb}_2\text{Ti}_2\text{O}_7$, at ambient pressure and in zero applied magnetic field, is known to remain a cooperative paramagnet to temperatures as low as 20 mK^{9,10,11}. In some studies, indications of spin freezing, or ordering of an undetermined nature, have been observed at temperatures as high as 1 to 2 K^{12,13,14}, however most of the magnetic spectral weight remains dynamic in frequency and diffuse in \mathbf{Q} -space to the lowest temperatures measured^{9,10,11}. The absence of order is quite enigmatic, as best estimates appropriate to $\text{Tb}_2\text{Ti}_2\text{O}_7$ and arising from Eq. 1 suggest a $\mathbf{Q}=0$ non-collinear Néel state below ~ 1 K^{5,7}.

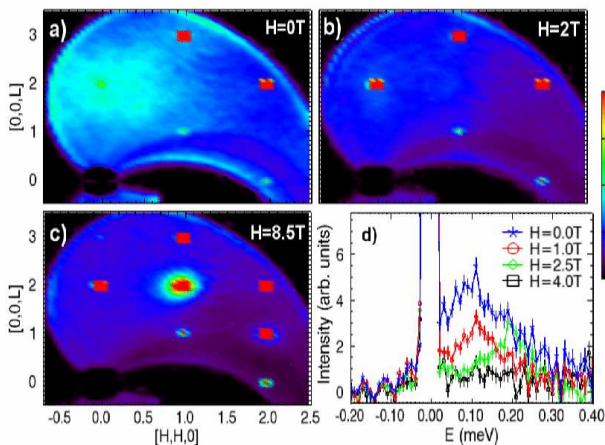


FIG. 1: Neutron Scattering for $-0.5 \text{ meV} < \hbar\omega < 0.5 \text{ meV}$, and within the (H,H,L) plane of $\text{Tb}_2\text{Ti}_2\text{O}_7$ at $T=1 \text{ K}$ is shown for (a) $H=0 \text{ T}$, (b) $H=2 \text{ T}$ and (c) $H=8.5 \text{ T}$. Panel d) shows high energy resolution scattering at $T=0.1 \text{ K}$, integrated in \mathbf{Q} and including the $(0,0,2)$ position. The quasi-elastic scattering extends to $\sim 0.25 \text{ meV}$ and it is dramatically diminished in fields as low as 1 T .

Earlier studies have shown that external perturbation by pressure and magnetic field may induce order in $\text{Tb}_2\text{Ti}_2\text{O}_7$. Neutron studies on $\text{Tb}_2\text{Ti}_2\text{O}_7$ in the presence of $[111]$ magnetic fields show an increase to the scattering at nuclear allowed Bragg positions¹⁵. More recently, the application of hydrostatic pressure on powder samples, as well as combinations of hydrostatic and uniaxial pressure, in concert with applied magnetic fields on single crystals show the existence of a magnetically-ordered state at low temperatures and field^{16,17}. In addition, recent measurements on polycrystalline $\text{Tb}_2\text{Ti}_2\text{O}_7$ in a relatively strong magnetic field shows evidence for very slow spin relaxation at temperatures as high as $10 - 20 \text{ K}$ ¹⁸. In this letter, we report new high resolution time-of-flight neutron measurements on a single crystal $\text{Tb}_2\text{Ti}_2\text{O}_7$ in a magnetic field applied along a $[110]$ direction. These measurements reveal a complex magnetic field - temperature phase diagram, characterized by the well known cooperative paramagnet, a polarized paramagnet, and a high field long range ordered magnetic phase with accompanying spin wave excitations.

The single crystal sample was grown by floating zone image furnace techniques and was cylindrical in shape with approximate dimensions of 2 cm long by 1 cm in diameter. It is the same high quality single crystal studied previously¹⁹. Time-of-flight neutron scattering measurements were performed using the Disk Chopper Spectrometer (DCS) at the NIST Center for Neutron Research²⁰. The DCS uses choppers to create pulses of monochromatic neutrons whose energy transfers on scattering are determined from their arrival times in the instrument's 913 detectors located at scattering angles

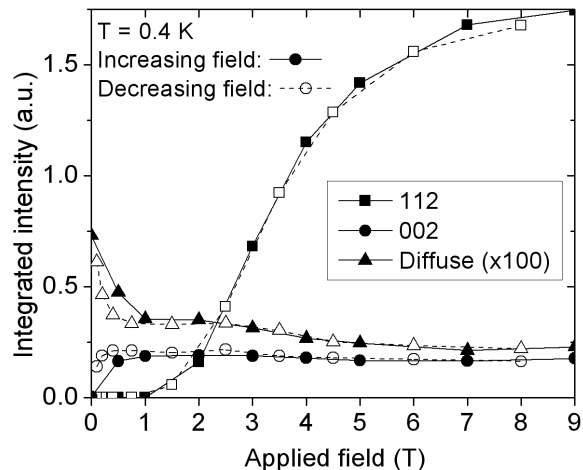


FIG. 2: The integrated intensity of the $(1,1,2)$ and $(0,0,2)$ Bragg peaks as a function of H at $T=0.4 \text{ K}$ are shown, along with the integrated quasi-elastic scattering making up the diffuse scattering. Note the complementarity of the $(0,0,2)$ Bragg scattering and the diffuse scattering and that both exhibit hysteresis with field.

from -30 to 140 degrees. Measurements were performed with 5 and 9 \AA incident neutrons.

Figure 1a, b, and c show reciprocal space maps in the (H,H,L) plane, integrating over $-0.5 < \hbar\omega < 0.5 \text{ meV}$ and taken at $T=1 \text{ K}$. These data employed 5 \AA incident neutrons. Figure 1a shows data in zero applied field, while Figs 1b and c show data in $H=2 \text{ T}$ and 8.5 T respectively. The data in Fig. 1a, in zero field, reproduce earlier neutron measurements⁹ of the “checkerboard” diffuse scattering, characteristic of very short range spin correlations - over single tetrahedra, which is particularly pronounced around $(0,0,2)$. Nuclear Bragg peaks allowed by the $Fd\bar{3}m$ pyrochlore space group are easily observed at $(3,1,1)$, $(2,2,2)$, $(1,1,1)$, and $(2,2,0)$. In addition a very weak Bragg peak is evident on close examination of the data at $(0,0,2)$ which is *not* allowed by the $Fd\bar{3}m$ space group. If nuclear in origin, its presence indicates $\text{Tb}_2\text{Ti}_2\text{O}_7$ is not a perfect cubic pyrochlore.

Figures 1b and c show the appearance of Bragg peaks on application of a $[110]$ magnetic field. At 2 T , the map shows the diffuse scattering around $(0,0,2)$ has largely disappeared, and a strong Bragg peak is evident at $(0,0,2)$. At higher fields there is clearly a transition to an ordered state, as the data at 8.5 T in Fig. 1c show the appearance of a set of new, intense Bragg peaks at most of the integer (H,H,L) positions in the field of view.

Measurements with 5 \AA incident neutrons and high resolution measurements using 9 \AA neutrons show the diffuse scattering around $(0,0,2)$ to be quasi-elastic in nature with a characteristic extent in energy of $\sim 0.25 \text{ meV}$. This is seen most clearly in Fig. 1d, which shows \mathbf{Q} -integrated scattering near $(0,0,2)$ as a function of en-

ergy at $T=0.1$ K and several values of magnetic field applied along the $[110]$ direction.

Parametric studies of the Bragg features at $(0,0,2)$ and $(1,1,2)$, as well as of the diffuse scattering near $(0,0,2)$ as a function of field and temperature were carried out to elucidate the new phase diagram for $\text{Tb}_2\text{Ti}_2\text{O}_7$ in a $[110]$ magnetic field. Figure 2 shows the integrated intensity of the $(0,0,2)$ and $(1,1,2)$ Bragg peaks, and the diffuse scattering near $(0,0,2)$ at $T=0.4$ K. These data were acquired from a set of seven scans, comprising a 3 degree sample rotation, and going through either the $(0,0,2)$ or $(1,1,2)$ Bragg positions. The $(0,0,2)$ integrated Bragg intensity rises almost immediately from a very small value and saturates beyond ~ 0.5 T. The diffuse scattering shows the complementary behavior, with a rapid fall off with increasing field, and then a leveling out at a small but non-zero intensity. At higher fields the diffuse scattering drops off again, near 5 T, to background. Measurements were made in both increasing and decreasing magnetic field, and hysteresis is observed in both the $(0,0,2)$ Bragg and diffuse scattering intensity.

The $(1,1,2)$ integrated Bragg intensity undergoes a sharp ‘‘S-shaped’’ rise from zero starting near 2 T and saturates near 8 T. No hysteresis is observed in its field dependence. The diffuse scattering appears to decrease in intensity to zero as the $(1,1,2)$ Bragg intensity goes through its inflection point near 5 T.

Figure 3 shows the temperature dependence of both the $(0,0,2)$ and $(1,1,2)$ Bragg peaks in magnetic fields of 1 and 7 T. As seen in Fig. 2, the $(1,1,2)$ Bragg peak has zero intensity in a field of 1 T. In an $H=7$ T field its intensity falls off sharply with downwards curvature, indicating a phase transition near $T_N \sim 3$ K. In striking contrast, the $(0,0,2)$ Bragg peak in an $H=1$ T field falls off with increasing temperature, but remains non-zero to temperatures at least as high as 24 K. The upwards-curvature associated with the $(0,0,2)$ T -dependence suggests no phase transition occurs in this temperature range. As can also be seen in Fig. 3, the $(0,0,2)$ intensity in $H=7$ T undergoes an anomaly at T_N , but remains large to at least 20 K.

The phase boundary between the high field ordered magnetic state and the polarized paramagnetic state is shown in the inset of Fig. 3. This line of phase transitions is identified from the time-of-flight neutron results of the form shown in Figs. 2 and 3, along with complementary triple axis neutron measurements and ac-susceptibility measurements²¹.

Time-of-flight measurements taken at a single sample orientation within the (H,H,L) plane and integrating along $(H,H,0)$ are shown in Fig. 4. These measurements, taken at $T=0.4$ K, approximate the inelastic scattering spectrum within the $(0,0,L)$, $-\hbar\omega$ plane around $(0,0,2)$. The four panels show data in Fig. 4a) zero magnetic field, b) $H=1$ T, c) $H=2$ T, and d) $H=3$ T. The zero field results show a quasi-elastic spectrum at energies

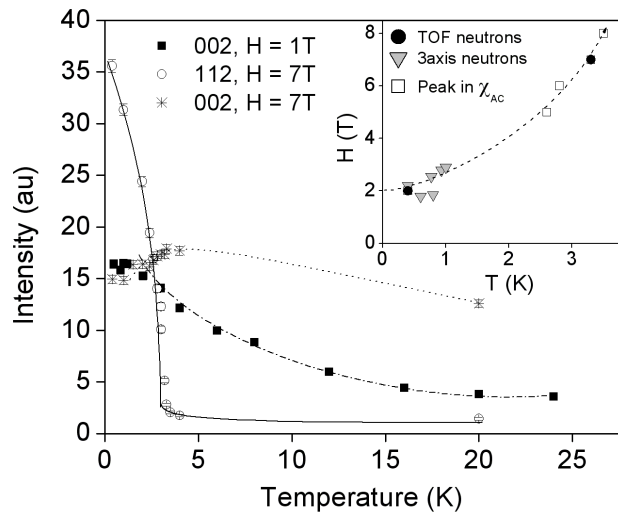


FIG. 3: The temperature dependence of the $(1,1,2)$ Bragg peak in $H=7$ T, as well as the $(0,0,2)$ Bragg peak in $H=1$ T and 7 T is shown. The inset shows the phase diagram for the magnetically long range ordered state in $\text{Tb}_2\text{Ti}_2\text{O}_7$, as determined by time-of-flight and triple axis neutron scattering and by ac-susceptibility measurements. All lines shown are guides-to-the-eye.

less than ~ 0.3 meV responsible for the diffuse scattering around $(0,0,2)$ and a gap in the 0.3 - 0.8 meV region. At higher energies we observe the same inelastic modes seen previously⁹, a relatively broad distribution of inelastic scattering from 0.8 meV to 1.8 meV, with a minimum in the dispersion around $(0,0,2)$. On application of an $H=1$ T field, sufficient to generate the full Bragg intensity at $(0,0,2)$ (see Fig. 2), the inelastic scattering is qualitatively similar to that in zero field, although the quasi-elastic diffuse scattering appears weaker and the inelastic bands of scattering between 0.8 meV and 1.8 meV are somewhat narrower.

At $H=2$ and 3 T, shown in Fig. 4c) and d), the spectrum is qualitatively different than that at the lower applied fields. Most strikingly, we observe sharp, dispersive spin wave excitations, which appear to have minima in their dispersion near $(0,0,1)$ and $(0,0,3)$. In addition the quasielastic scattering that was responsible for the ‘‘checkerboard’’ of diffuse scattering in zero field, is now clearly resolved as a relatively dispersionless inelastic mode at $\hbar\omega \sim 0.3$ meV. The higher energy inelastic scattering is resolved into relatively narrow energy bands. As seen in Fig. 2, this new magnetic inelastic spectrum occurs within the magnetically ordered phase, characterized by the strong $(1,1,2)$ Bragg peak.

We identify the $(0,0,2)$ Bragg peak, which appears on application of a very small applied field as a signature of a polarized paramagnet. We do so based on two observations: i) the absence of a clear signature of a phase transition associated with the $(0,0,2)$ intensity in an $H=1$

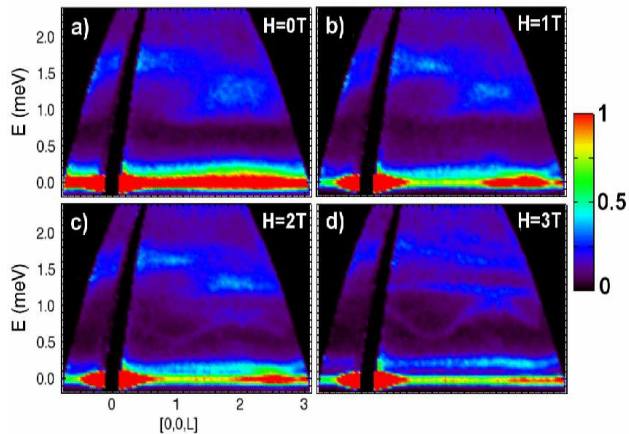


FIG. 4: Neutron scattering data within the $(0,0,L)$ - energy plane at $T=0.4$ K and a) $H=0$, b) $H=1$ T, c) $H=2$ T, and d) $H=3$ T are shown.

T field below 24 K; and ii) the absence of collective spin wave excitations at $H=1$ T, as are observed at higher fields.

The Tb sites in the pyrochlore structure can be thought of as lying on two sets of chains oriented along orthogonal $[1,1,0]$ directions. The application of a magnetic field along one particular $[1,1,0]$ is expected to polarize half of the Tb sites, such that moments on chains parallel to the field direction point align along the local $[1,1,1]$ direction with a component parallel to the field. Such a polarized paramagnet displays magnetic Bragg peaks at the $(0,0,2)$ positions as well as the nuclear Bragg positions of the $Fd\bar{3}m$ space group: $(3,1,1)$, $(2,2,2)$, $(1,1,1)$, and $(2,2,0)$, as observed experimentally in Fig. 1c). This state is neither expected to display a phase transition, nor to support spin waves, as the long range correlations responsible for the magnetic Bragg

peaks are due to a single-ion canting of a subset of the moments along the applied field direction.

In contrast, the high field magnetically ordered state shows both a phase transition near $T_N \sim 3$ K, and well defined spin wave excitations. The dispersive spin wave excitations appear to be incompatible with a hard Ising-like $(1,1,1)$ anisotropy for the spins, and require continuous spin degrees of freedom. Similar issues had arisen in understanding the “checkerboard” pattern of diffuse scattering in $H=0$ ^{9,22}.

The detailed magnetic structure of the high field ordered phase will be reported on separately. However, as seen in Fig. 1c) new Bragg peaks are seen at all (H,H,L) indices within the field of view except $(0,0,1)$. This pattern of observed reflections, although not the detailed relative intensities, is similar to the low field antiferromagnetic state reported by Mirebeau et al.^{16,17} in $Tb_2Ti_2O_7$ under application of both a uniaxial and a hydrostatic applied pressure. This suggests that these two long range ordered states are related, and that the appearance of an ordered state at high fields under ambient pressure may be due to strong magnetoelastic effects, as have been reported in $Tb_2Ti_2O_7$ ²³.

We hope these results for a new phase diagram for $Tb_2Ti_2O_7$ at ambient pressure, and the results for the spin wave spectrum within the magnetically ordered phase motivate a complete understanding of the complex and exotic ground state of this geometrically frustrated magnet.

We wish to acknowledge useful contributions from M.J.P. Gingras, G. Luke and J. Rodriguez. This work was supported by NSERC of Canada, and utilized facilities supported in part by the NSF under Agreements DMR-9986442 and DMR-0086210 and by the U.S. Department of Energy under contracts DE-AC02-98CH10886.

¹ see, for example: **Frustrated Spin Systems**, edited by H.T. Diep (World Scientific Publishing Co. Pte. Ltd., Singapore, 2004).

² J.N. Reimers, Phys. Rev. B, **45**, 7287 (1992).

³ R. Moessner and J.T. Chalker. Phys. Rev. B **58**, 12049, (1998).

⁴ M.J. Harris, M.P. Zinkin, Z. Tun, B.M. Wanklyn and I.P. Swainson. Phys. Rev. Lett. **73**, 189 (1994).

⁵ B.C. den Hertog, and M.J.P. Gingras, Phys. Rev. Lett. **84**, 3430 (2000).

⁶ M.J. Harris, S.T. Bramwell, D.F. McMorrow, T. Zeiske and K.W. Godfrey. Phys. Rev. Lett. **79**, 2554-2557, (1997).

⁷ M.J.P. Gingras, B.C. den Hertog, M. Faucher, J.S. Gardner, S.R. Dunsiger, L.J. Chang, B.D. Gaulin, N.P. Raju and J.E. Greedan, Phys. Rev. B **62**, 6496 (2000).

⁸ S. Rosenkranz, A.P. Ramirez, A. Hayashi, R.J. Cava, R.

Siddharthan and B.S. Shastry. J. App. Phys. **87**, 5914 (2000).

⁹ J.S. Gardner, B.D. Gaulin, A.J. Berlinsky and P. Waldron, S.R. Dunsiger, N.P. Raju, and J.E. Greedan, Phys. Rev. B **64**, 224416 (2001).

¹⁰ J.S. Gardner, S.R. Dunsiger, B.D. Gaulin, M.J.P. Gingras, J.E. Greedan, R.F. Kiefl, M.D. Lumsden, W.A. MacFarlane, N.P. Raju, J.E. Sonier, I. Swainson and Z. Tun. Phys. Rev. Lett. **82**, 1012 (1999).

¹¹ J.S. Gardner, A. Keren, G. Ehlers, C. Stock, E. Segal, J.M. Roper, B.Fåk, M.B. Stone, P.R. Hammar, D.H. Reich and B.D. Gaulin. Phys. Rev. B **68**, 180401 R1-4, (2003)

¹² Y. Yasui, M. Kanada, M. Ito, H. Harashina, M. Sato, H. Okumura, K. Kakurai and H. Kadowaki. J. Phys. Soc. Jap. **71**, 599 (2002).

¹³ S.R. Dunsiger, R.F. Kiefl, J.A. Chakhalian, K.H. Chow, J.S. Gardner, J.E. Greedan, W.A. MacFarlane, R.I. Miller,

- G.D. Morris, A.N. Price, N.P. Raju and J.E. Sonier. *Physica B* **326**, 475 (2003).
- ¹⁴ N. Hamaguchi, T. Matsushita, N. Wada, Y. Yasui, and M. Sato, *Phys. Rev. B*, **69**, 132413 (2004).
- ¹⁵ Y. Yasui, M. Kanada, M. Ito, H. Harashina, M. Sato, H. Okumura and K. Kakurai. *J. Phys. Chem. Sol.* **62**, 343 (2001).
- ¹⁶ I. Mirebeau, I.N. Goncharenko, *J. Phys.: Condensed Matter* **17**, S771 (2005).
- ¹⁷ I. Mirebeau, I.N. Goncharenko, G. Dhahlenne and A. Revcolevschi, *Phys. Rev. Lett.* **93**, 187204 (2004).
- ¹⁸ B.G. Ueland, G.C. Lau, R.J. Cava, J.R. O'Brien, and P. Schiffer, *Phys. Rev. Lett.*, **96**, 027216 (2006).
- ¹⁹ J.S. Gardner, B.D. Gaulin and D. McK Paul. *J. Crys. Growth* **191**, 740 (1998).
- ²⁰ J.R.D. Copley and J.C. Cook, *Chem. Phys.*, **292**, 477 (2003).
- ²¹ J. Rodriguez and G.M. Luke, unpublished.
- ²² Y.J. Kao, M. Enjalran, A. Del Maestro, H.R. Molavian, and M.J.P. Gingras, *Phys. Rev. B*, **68**, 172407 (2003).
- ²³ I.V. Aleksandrov, B.V. Lidskii, L.G. Mamsurova, M.G. Neigauz, K.S. Pigal'skii, K.K. Pukhov, N.G. Trusevich and L.G. Scherbakova, *JEPT* **62**, 1287 (1985); L.G. Mamsurova, K.S. Pigal'skii and K.K. Pukhov, *JETP Lett.*, **43**, 755 (1986).